Accumulation of defense systems drives panphage resistance in *Pseudomonas aeruginosa*

Ana Rita Costa[1,2,#], Daan F. van den Berg[1,2,#], Jelger Q. Esser[1,2,#], Aswin Muralidharan[1,2], Halewijn van den Bossche[1,2], Boris Estrada Bonilla[1,2], Baltus A. van der Steen[1,2], Anna C. Haagsma[1,2], Franklin L. Nobrega[3], Pieter-Jan Haas[4], Stan J.J. Brouns[1,2,*]

[1] Department of Bionanoscience, Delft University of Technology, 2629 HZ Delft, Netherlands

[2] Kavli Institute of Nanoscience, Delft University of Technology, 2629 HZ Delft, Netherlands

[3] School of Biological Sciences, University of Southampton, SO17 1BJ Southampton, United Kingdom

[4] Medical Microbiology, University Medical Center Utrecht, Utrecht University, 3584 CX Utrecht, Netherlands

[#] These authors contributed equally.

* Correspondence: stanbrouns@gmail.com

Abstract

Prokaryotes carry multiple distinct anti-viral defense systems. However, the impact of carrying a multitude of defense systems on virus resistance remains unclear, especially in a clinical context. Using a collection of antibiotic-resistant clinical strains of *Pseudomonas aeruginosa* and a broad panel of phages, we demonstrate that intracellular defense systems are major determinants of phage host range and that overall phage resistance scales with the number of defense systems in the bacterial genome. We show that individual defense systems are specific to certain phage types, including Jumbo phages, and that the accumulation of defense systems with distinct specificities results in panphage resistant phenotypes. Accumulation of defense systems is aided by their localization within mobile phage defense elements facilitating horizontal gene transfer. Overall, we show that panphage resistant, defense-accumulating strains of *P. aeruginosa* with up to 19 phage defense systems already occur in the clinic, which may impact the development of phage-based therapeutics.

Keywords: Phage defense systems, *Pseudomonas aeruginosa*, panphage resistance, Jumbo phage, defense island

Bacteriophage predation imposes a strong evolutionary pressure on bacteria to evolve phage defense mechanisms[1]. Several ways to defend against phages have previously been discovered, including receptor modification on the cell surface[2,3], and intracellular defenses[4-6] such as CRISPR-Cas[7,8] and Restriction-Modification[9,10].

More recently, dozens of previously unknown innate immune systems have been discovered based on the observation that immune systems cluster in defense islands[11-16]. The presence and defense system composition of these defense islands are highly variable among individual strains[4,15,17], and strongly contribute to phage-host co-evolution in natural populations[1]. The presence of multiple variable defense systems in bacterial genomes raises the important question what the impact is of all these immune systems on overall phage resistance of bacterial pathogens.

To address this question, we assembled a set of 17 clinical, antibiotic-resistant *Pseudomonas aeruginosa* strains and isolated a custom panel of 28 phages from 10 phylogenetic groups. We then analyzed the infectivity of the strains across the panel of phages. This revealed that intracellular phage defense mechanisms are a major determinant of the phage susceptibility of *P. aeruginosa*, and that strains rich in phage defense systems are inherently more resistant. One strain contained 19 anti-phage defense systems and displayed a panphage-resistant phenotype, in addition to having an extended drug-resistant (XDR) phenotype. Our data further revealed that defense systems are specific to certain phage types, such as Jumbo phages, and are almost always encoded in mobile genetic elements to facilitate exchange among strains via horizontal gene transfer. Overall, our findings have broad implications for our understanding of phage defense and the development of phage-based antibacterial therapeutics, as the widespread use of phages may select for naturally occurring panphage-resistant phenotypes in clinical, antibiotic-resistant strains.

Results

Defense systems are abundant and diverse in clinical *P. aeruginosa* strains

To determine if our set of 17 antibiotic-resistant clinical strains is representative of the diversity and abundance of defense systems in the *P. aeruginosa* species as a whole, we compared the prevalence of defense systems in our collection to 315 complete genomes of *P. aeruginosa* from the Refseq database. The *P. aeruginosa* genomes from the database carry 70% (117/166) of the known defense system subtypes (**Fig. 1a**, **Supplementary Table 1**), providing a large and diverse defense arsenal similar to that found in our clinical isolates (**Supplementary Table S2**). The number of defense systems per genome ranged between 1

and 19 systems for both database (median of 7, **Fig. 1b**) and clinical strains (median of 8, **Fig. 1d**). This is in line with recent observations that *P. aeruginosa* has one of the most diverse arsenals of anti-phage defense[17]. Overall, we demonstrate that *P. aeruginosa* genomes encode multiple and diverse anti-phage defense systems, and establish that our collection of clinical isolates is representative of the *P. aeruginosa* species as a whole in both defense system diversity and number.

Accumulation of defense systems provides increased phage protection

To obtain a relevant panel of phages, we used our set of clinical *P. aeruginosa* strains as hosts to enrich and isolate 28 different phages from sewage water (**Supplementary Table 3**). A phylogenetic analysis and electron microscopy showed that the phage panel is composed of *Caudoviricetes* (dsDNA tailed phages), with 13 podophages (5 *Autographiviridae*, 3 *Bruynoghevirus*, 1 *Litunavirus*, 1 *Paundecimvirus*, and 3 unknown), 5 siphophages (1 *Samunavirus* and 4 unknown), and 10 myophages (9 *Pbunavirus* and 1 *Phikzvirus*, a Jumbo myophage related to nucleus-forming *Pseudomonas* phage phiKZ[18]).

To determine the effect of the defense systems on the susceptibility of the clinical strains to our panel of phages, we first assessed the ability of the phages to adsorb and infect the strains, or to only adsorb to their cell surface. Out of a total of 504 phage-host combinations (28 phages times 18 hosts), 307 phage-host combinations resulted in no infection (**Fig. 2a**). We hypothesize that non-infection can occur in two ways: the phage either fails to adsorb to the cell surface (i.e. no receptor), or phage propagation is unsuccessful, possibly by the action of anti-phage defense. From adsorption assay data we derived that out of the 307 non-infection cases, 37% (114) could be attributed to failed adsorption, leaving 63% (193) of the phage-host combinations where action of internal defenses is expected.

Importantly, we detected a strong correlation between the number of defense systems carried by a strain and the extent of phage resistance, with each system increasing the resistance on average 4% (Linear regression model, p-value = 4.2e-4, adjusted R-squared = 0.52) (**Fig. 2b**). Supporting this correlation, the two strains with most defense systems in our collection, L0872 (19 defense systems) and K6024 (17 defense systems) are the most insensitive to phage infection (**Fig. 2a**,**c**), with L0872 showing a panphage-resistant phenotype (i.e. not infected by any phage). Strikingly, strain L0872 is additionally resistant to 12 of 14 antibiotics tested (**Supplementary Table 2**), suggesting co-occurring antibiotic and phage resistance.

In summary, we show that phage defense systems are major determinants of the phage sensitivity profiles of strains, and thus of phage host range. The accumulation of defense

systems in genomes strongly correlates to overall resistance to infection by phages. We also observe that *P. aeruginosa* strains that are very resistant and extensively drug-resistant (XDR) already exist in clinical settings, and can cause infections that are exceptionally challenging to treat.

Adaptive immunity impacts susceptibility to temperate phages

Approximately 35% (6/17) of the clinical strains contain adaptive immune systems in the form of CRISPR-Cas Type I-F. To investigate the contribution of CRISPR-Cas to phage resistance we identified all spacers targeting our phage panel and assessed their potential effect on the phage host range. We detected 24 unique spacers matching our phage panel, among which 20 are interference-proficient (i.e. spacers with matching protospacer adjacent motif (PAM) and protospacer) and 4 are priming-proficient (i.e. spacers with a ±1 slipped PAM[19] or up to 5 protospacer mutations[20,21]) (**Supplementary Table 4**). These spacers were distributed over six strains (white and blue circles in **Fig. 2a**). Interestingly, 23 of the 24 spacers target temperate phages (ϕPa19, ϕPa42, and ϕPa47), and only one spacer matches a virulent phage (ϕPa8). This is in line with previous findings that spacers of *P. aeruginosa* mostly match temperate phages[22]. Strains with matching spacers were able to limit infection by phages ϕPa42 and ϕPa47, but not phage ϕPa19 (**Fig. 2a**). No known anti-CRISPR (Acr) genes[23] were found in ϕPa19, suggesting that an unknown Acr might be responsible for CRISPR evasion by ϕPa19[24].

Overall, our results suggest that CRISPR-Cas type I-F contributes to resistance of the clinical strains against temperate phages but plays a minor role against the vast majority of virulent phages in the panel. Although the catalog of spacers may evolve through CRISPR adaptation, it suggests that the current set of spacers does not explain the infection profiles.

Innate defense systems provide anti-phage activity against specific phage morphotypes

To understand the contribution of individual innate defense systems to the observed broad-spectrum phage immunity, we cloned 15 defense systems (**Supplementary Fig. 1a**) found in the *P. aeruginosa* clinical isolates into the low-copy plasmid pUCP20[25], under control of their native promoters. The plasmids were introduced into *P. aeruginosa* strain PAO1, which is infected by 17 phages of our panel. We validated that the defense systems represent no burden or toxicity to cell growth (**Supplementary Fig. 1b**), and subsequently assessed the

defense-containing PAO1 strains for changes in phage susceptibility using efficiency of plating (EOP) and bacterial culture collapse assays.

The EOP (**Fig. 3a**) and bacterial culture collapse (**Fig. 3b**) assays show that QatABCD, CBASS Type II-C, CBASS Type III, and Zorya Type I have broad activity against our panel of phages. The other 11 defense systems have morphotype-specific activities, targeting one (myophage-specific Druantia Type III and IetAS) or two phage morphotypes. This is in line with the sensing of specific conserved phage proteins, such as the capsid or terminase proteins, to trigger an immune response[26-28].

The bacterial culture collapse assays provided additional information about the mechanisms of antiviral activity of the defense systems. We observed that TerY-P protects using mechanisms that do not require suicide of the infected cell, as protection of the culture is observed even at high multiplicity of infection (MOI) (**Fig. 3b**), and most cells survive in microscopy assays using propidium iodide (**Fig. 3c**). By contrast, the anti-phage effects of QatABCD, RADAR, CBASS type III, II-A and II-C, HerA_DUF4297 (system 20[29]), Druantia Type III, AVAST Type V, Gabija, AbiE, IetAS, and Septu Type I all seem to result from a mechanism of abortive infection, in which the infected cell is likely sacrificed to protect the bacterial population[30]. Surprisingly, Wadjet Type I, which previously showed only anti-plasmid activity[31], also displayed an abortive infection phenotype against different phages, including Jumbo ϕPa36 (**Fig. 3a,b, Supplementary Fig. 1c**). Here we separated the abortive infection phenotype in classic and population-wide abortive infection. The classic abortive infection phenotype is characterized by bacterial culture collapse at high phage MOI but growth at low MOI, whereas population-wide abortive infection appears as culture collapse (more abrupt than for control cells) at both phage MOIs (**Fig. 3b**). We confirmed the population-wide abortive infection to be a form of anti-phage defense by following phage concentration over time in infected cultures of PAO1 containing the defense system and observed a decrease in phage production in the defense strain relative to the control strain (**Supplementary Fig. 1c**). We speculate that the culture collapse observed at low MOI in the population-wide abortive infection phenotype could be the result of some form of communication among cells[32,33], which transmits the infection signal to non-infected cells and may induce population wide suicide.

For Zorya Type I we detect mechanisms of defense that result in either normal growth or abortive infection depending on the phage morphotype. For example, while cells containing Zorya Type I show normal growth when infected by podo- and siphophages (**Fig. 3b**,**c**), an abortive infection phenotype is observed against myophages (**Fig. 3b**). This suggests that this defense system employs conditional abortive infection mechanisms, in which abortive

infection is triggered only upon failure of a first response that potentially targets the phage leaving the cell unharmed.

In summary, we show that individual defense systems have anti-phage activities specific to certain phage morphotypes. The vast majority (14/15) of the defense systems tested operate via abortive infection, with one defense system utilizing a conditional antiviral mechanism that supports either normal growth or triggers abortive infection depending on the type of phage.

Jumbo phage infection is blocked by CBASS Type III and AVAST Type V

In addition to Wadjet Type I discussed earlier, we show that CBASS Type III and AVAST Type V systems provide robust (>10^5-fold) protection against infection by phiKZ-like, nucleus-forming Jumbo phage ϕPa36, stronger than for any other phage in our panel. Jumbo phages are known to produce a nuclear shell[34] that shields phage DNA during replication from DNA-targeting systems such as RM and CRISPR-Cas systems[35,36]. This suggests that CBASS Type III and AVAST Type V do not exert their anti-phage activity via direct DNA sensing or targeting, and instead may act on protein level (AVAST Type V)[26,29] or via induction of abortive infection upon sensing of a phage protein (CBASS Type III)[27]. Our results demonstrate that while Jumbo phages have developed specific mechanisms to counteract DNA-targeting defense systems, other defense systems have evolved a specificity that is effectively targeting Jumbo phages.

Infectivity profiles of the clinical strains correspond to specificities of individual defense systems

To relate the combined effect of individual phage defense systems (**Fig. 3**) to the overall phage protection observed in the genetically inaccessible clinical strains (**Fig. 2**), we looked at the phage susceptibility profile of the clinical strains and cross-checked the susceptibility patterns of PAO1 strains equipped with a single defense system. For this analysis, we considered only the defense systems that provided defenses higher than 10^4-fold reductions in EOP, because we expect these to produce measurable effects in the phage infectivity data in **Fig. 2**. Under these restrictions, we assessed the effect of QatABCD and RADAR on myophage, Zorya Type I on podo- and siphophage, CBASS Type II-C in siphophage, and CBASS Type III and AVAST Type V on Jumbo phage. We observe that the strains containing Zorya Type I (K6024) and AVAST Type V (L1171, L0213) have the expected phage resistance profile (**Supplementary Fig. 1d**). For the two strains containing CBASS Type II-C (L1347 and L1496), one (L1496) has the expected resistance against siphophages ϕPa15 and ϕPa28. For strains containing

CBASS Type III (L1264, L1361, L0665, K5993), all except L1264 are resistant to infection by Jumbo ϕPa36, as predicted. Surprisingly, we observe that the single strain (K6156) containing both QatABCD and RADAR is not resistant to infection by myophages, despite the strong protection provided by the individual systems in PAO1. Many other factors may explain the differences in the phage resistance profile of the clinical strains in comparison to those predicted by the EOP assays in PAO1, including defense systems being inactive in the clinical strain, prophage-encoded exclusion mechanisms, and the presence of anti-defense genes in the bacterial genomes.

To assess the impact of phage-encoded anti-defenses in the phage infectivity profile of the clinical strains, we searched for known anti-defenses in the phage genomes, including anti-RM[37-39], Acr[40], anti-CBASS[27,41], anti-Pycsar[41], and anti-TIR-STING[42] proteins. Only one anti-defense gene, anti-CBASS Type II (*acbII*) was found, in phage ϕPa48. This phage adsorbs to one of the two strains carrying a CBASS Type II-C system (L1496) and infects it productively, in contrast to all other podophages (**Fig. 2a,c**), supporting the idea that the anti-gene plays a role in overcoming host defenses. We also assessed the presence of anti-genes in the host genome and found an *acbII* in a prophage region in strain L1347, which also carries the CBASS Type II-C system in the chromosome, likely rendering the CBASS Type II-C system of the strain inactive. This would explain our previous observation that strain L1347 does not protect against siphophages ϕPa15 and ϕPa28, as would be expected from the EOP results obtained in PAO1 expressing the individual CBASS Type II-C defense system (**Fig. 3a**).

Overall, we observe the morphotype-specific activity of individual defense systems in PAO1 to corroborate the majority (7/10) of the phage resistance profile of clinical strains that contain multiple defense systems.

Defense systems co-localize to provide broad complementary protection

Based on the observation that defense systems provide distinct morphotype-specific anti-phage activities (**Fig. 3**), we hypothesized that specific combinations of defense systems may be beneficial to the cell by providing a complementary protective range, and would be a conserved feature in bacterial genomes to achieve broad antiviral specificity. To test this hypothesis, we assessed the co-occurrence (i.e. presence in the same genome) and co-localization of the defense systems found in *P. aeruginosa* genomes in the RefSeq database. We found multiple instances of co-occurrence (adjusted p-value < 0.01 & Pearson correlation ≥ 0.2) that suggest potential beneficial combinations, including pairs of systems tested here (**Fig. 4a**, **Supplementary Table 5**). Of the tested pairs, only the combination of Druantia Type III and TerY-P was almost always found to co-localize (25/26). These systems have

complementary morpho-specific targeting (**Fig. 3**), with Druantia Type III protecting from myophages and TerY-P from podophages. We further explored the existence of additional defense systems that co-occur and co-localize with this pair (within 50 genes for > 50% of the instances of co-occurrence, adjusted p-value < 0.05, and Pearson correlation ≥ 0.2), and found RM Type I, Mokosh Type I[13] and Wadjet Type I to frequently associate with the combination of Druantia Type III and TerY-P. While we do not have anti-phage activity information for RM Type I or Mokosh Type I, Wadjet Type I complements the specificity of Druantia Type III and TerY-P by targeting sipho and Jumbo phages (**Fig. 3**, **Fig. 4b**). Interestingly, these defense systems were found to be part of a large defense island located within a genomic integration hotspot (**Fig. 4c**). This defense island is composed of several phage defense elements (PDEs)[15] and is present in the most phage-resistant strain of our panel of clinical isolates (L0872, **Fig. 2**, **Fig. 4c**), supporting a potential role in broad phage defense. The defense island-mediated broad phage defense might be exchanged among clinical strains via horizontal gene transfer, as the same genomic integration hotspot is found in 95% of the RefSeq *P. aeruginosa* genomes analyzed here. The relevance of PDEs to the spread of phage resistance is further emphasized by the fact that 97.5% of all the defense systems identified in *P. aeruginosa* are encoded in PDEs, similar to the numbers previously reported for *Vibrio* species[1]. Overall, we demonstrate that defense systems co-occur and co-localize within defense islands and provide a complementary as well as overlapping range of anti-phage activities.

Discussion

Bacterial strains often carry numerous distinct phage defense systems in their genomes[17]. We found that *P. aeruginosa* strains carry at least 70% of the currently known defense systems, making this species a versatile bacterial model to study phage immunology. Using a diverse set of clinical isolates of *P. aeruginosa*, we show that the accumulation of defense systems in the genome results in broad and robust immunity against phage infection, with each defense system contributing an additional 4% to anti-phage defense.

By testing the activity of 15 defense systems against our phage panel, we show that defense systems have anti-phage specificity often associated with the phage morphotypes, suggesting that defense systems operate using conserved properties within phage phylogenetic groups. Interestingly, defense system co-occurrence and co-localization analysis revealed that Druantia Type III, TerY-P, Wadjet Type I, RM Type I, and Mokosh Type I are a conserved combination and present on a large defense island located in a genomic integration hotspot. We expect this conserved collection of defense systems to provide broad phage protection

via the complementary phage specificities of the individual defense systems. The complementary activities of naturally co-occurring defense systems have also been found to prevent plasmid dissemination in *Vibrio cholerae* El Tor strains[43], proposing an important role of the defense system cooperation to bacterial pathogenicity.

The overlapping specificity of defense systems provides the evolutionary option to select different sets of defense systems from the 117 subtypes present in the *P. aeruginosa* pangenome to achieve broad antiviral specificity. We observed four different combinations of phage defense systems in strains containing a total of 19 defense systems in the Refseq database, indicating the emergence of independent, phage-resistant lineages (**Supplementary Table 1**). Previously, the pan-immunity model[4] proposed that a single strain is unable to carry all defense systems due to fitness costs (e.g. auto-immunity, energy burden), but can acquire defense systems encoded by closely related strains via horizontal gene transfer. Supporting this idea, the clinical isolate from our collection that encodes 19 defense systems is panphage-resistant, including to commercially available *P. aeruginosa* phage cocktails. Attempts to isolate phages specifically against this strain from diverse wastewater samples or to transform plasmid DNA proved unsuccessful, again pointing to the strain's inherent ability to defend from incoming threats. The defense barrier itself may start limiting the further uptake of foreign genetic material by horizontal gene transfer, restricting the acquisition of additional defense systems.

Our extensive analysis of the native phage defense systems in *P. aeruginosa* revealed that some defense systems employ a conditional abortive infection mechanism that can protect the cell from infection by certain phages without causing growth arrest or cell death. A similar effect was previously reported for Septu Type I using different forms of methylated phage T4[44]. Moreover, Druantia Type III shows an abortive infection phenotype against our phage panel, but was described to have non-abortive infection activities against phage T4[44]. These observations are in line with a model that suggests that certain defense systems can utilize a layered antiviral activity, in which the defense first attempts to directly interfere with the phage life cycle, sacrificing the cell only when this fails.

Altogether, our results highlight the relevance of phage defense systems in defining phage susceptibility of cells and thus phage host range. While phage host range has traditionally been mostly linked to receptor-associated factors[45], we show that defense systems that act intracellularly are also a major defining factor of phage susceptibility. As phage defense-accumulating *P. aeruginosa* clinical strains occur naturally, we predict that panphage-resistant phenotypes may become more dominant with wider use of therapeutic phages, and may even acquire more defense systems by horizontal gene transfer as reported previously for *Vibrio*[1,15].

It is, therefore, crucial to monitor the evolution and dispersion of phage-resistant clinical pathogens and to select and engineer phages to overcome natural defenses through anti-defense genes.

Methods

Bacteria

A set of 17 clinical isolates of *P. aeruginosa* isolated at the University Medical Centre Utrecht (UMCU) (**Supplementary Table 2**) were used for phage isolation and characterization. *Escherichia coli* strain Dh5α was used to clone plasmid pUCP20 with individual defense systems. *P. aeruginosa* strains containing pUCP20 with individual defense systems were constructed from *P. aeruginosa* strain PAO1. All bacterial strains were grown at 37 °C in Lysogeny Broth (LB) with 180 rpm shaking for liquid cultures, or in LB agar (LBA) plates for solid cultures. Strains containing plasmid pUCP20 were grown in media supplemented with 100 µg/ml of ampicillin (for *E. coli*) or 200 µg/ml of carbenicillin (for *P. aeruginosa*).

Bacteriophages

Phages used in this study are described in **Supplementary Table 3**. All phages were isolated from sewage water. Approximately 1 ml of sewage sample was added to 20 ml of LB, inoculated with 100 µL of overnight cultures of each *P. aeruginosa* clinical isolate, and incubated overnight at 37 °C with 180 rpm shaking. Samples were centrifuged at 3,000 × *g* for 15 min and filter-sterilized (0.2 µm PES). The phage-containing supernatant was serially diluted in LB and spotted on double-layer agar (DLA) plates of the isolation strains for the detection of phages. Single plaques with distinct morphologies were picked with sterile toothpicks and spread with sterile paper strips onto fresh bacterial lawns. The procedure was repeated until a consistent plaque morphology was obtained. Phages from purified plaques were then produced in liquid media with their respective host, centrifuged, filter-sterilized, and stored as phage lysates at 4 °C. For EOP and liquid infection assays (see below), phage stocks were obtained from lysates prepared on PAO1 and their concentration normalized to ≈$1x10^8$ pfu/ml.

Phage host range

Phages were 10-fold serially diluted in LB and spotted onto DLA plates containing each *P. aeruginosa* clinical strain. The plates were incubated overnight at 37 °C and the phage plaques were observed to distinguish productive infection (lysis with individual phage plaques formed)

from lysis from without[46] (lysis without individual phage plaques). The infectivity of phage cocktails was tested in *P. aeruginosa* strain L0872 following the same protocol.

Adsorption assays

Early-exponential (optical density at 600 nm, OD_{600} ≈ 0.3) cultures of the *P. aeruginosa* clinical isolates were added in triplicates to the wells of 96-well plates. Phages were added to these cultures at an MOI of 0.01 and incubated at 37 °C with 100 rpm shaking for 15 min. The plates were centrifuged and a sample of the supernatant was taken, 10-fold serially diluted, and plated onto DLA plates of PAO1 to determine the titer of phages that did not adsorb to the clinical strain. A control plate in which phages were added to LB was used to determine the total phage concentration. The concentration of adsorbed phages was determined by subtracting non-adsorbed phage concentration from the total phage concentration in the suspension. The percentage of adsorbed phages was calculated as the ratio between adsorbed phages and total phages. Phage adsorption was categorized as strong adsorption when higher than 70%, and weak adsorption when between 50% and 70%.

Transmission electron microscopy

One mL of each phage lysate at >10^9 pfu/mL was pelleted at 21,000 × *g* for 1 h, washed, and re-suspended in 1 mL of MilliQ water. Phages (3.5 µL) were deposited and incubated for 1 min on TEM grids (Carbon Type-B 400 mesh, TED PELLA). Grids were washed three times with 40 µL of MilliQ water and stained with 3.5 µL of 2% (w/v) uranyl acetate (pH 4.0) for 30 seconds. Grids were examined using a JEM-1400 plus (JEOL) TEM.

Extraction of phage DNA and bacterial DNA

Phage DNA was extracted using phenol-chloroform. For this, 5 mL of each phage lysate at >10^9 pfu/mL were treated with 1 µg/mL of DNase I and RNase for 30 min. Ethylenediaminetetraacetic acid (EDTA), proteinase K, and sodium dodecyl sulfate (SDS) were added to the sample at final concentrations of 20 mM, 50 µg/mL, and 0.5% respectively, and the samples were incubated at 56 °C for 1 h. The samples were then mixed with an equal volume of chloroform and centrifuged at 3,000 × *g* for 10 min. The aqueous phase was recovered and the procedure was repeated sequentially with a 1:1 mixture of phenol:chloroform, and chloroform. The resulting aqueous phase was mixed with 0.1 volume of sodium acetate 3M (pH 5) and 2.5 volumes of ice-cold absolute ethanol and incubated at -20 °C overnight. The extracted DNA was pelleted at 14,000 × *g* for 15 min and washed in ice-cold 70% ethanol, before re-suspending in ultrapure water. Bacterial genomic DNA was extracted using the GeneJET Genomic DNA Purification kit (Thermo Fisher). The quality and

quantity of extracted phage and bacterial DNA were estimated using a NanoPhotometer and a Qubit fluorometer, respectively.

Phage sequencing

For samples sequenced at Beijing Genomics Institute (BGI) (**Supplementary Table 3**), the phage genomic DNA was fragmented by Covaris 55 µL series Ultrasonicator, and used to construct DNA nanoball (DNB)-based libraries by rolling circle replication. DNA was sequenced using the BGI MGISEQ-2000 platform (BGI Shenzhen, China) with a paired-end 100 nt strategy, generating 4.6-19.2 Gb sequencing data for each sample. For phage samples sequenced in-house, phage DNA was fragmented by Covaris M220 Focused-Ultrasonicator, and libraries were prepared using the NEBNext Ultra II DNA Library Prep Kit. Size distribution was checked on an Agilent D1000 Screen Tape System, and the libraries were pooled equally and spiked with approximately 5% of the PhiX control library. The pooled library was sequenced with an Illumina MiSeq using the MiSeq Reagent Nano Kit v2 (500-cycles). For samples sequenced at the Microbial Genome Sequencing Center (MiGS, Pittsburgh, PA, USA), sample libraries were prepared using the Illumina DNA Prep kit and IDT 10 bp UDI indices, and sequenced on an Illumina NextSeq 2000, producing 2x151 bp reads. Demultiplexing, quality control, and adapter trimming were performed with bcl-convert (v3.9.3). Reads obtained for all samples were assembled using Unicycler v0.5.0[47]. For samples sequenced in-house, the control PhiX was manually removed from the assembled contigs using Bandage[48].

Bacterial sequencing

For samples sequenced at BGI (**Supplementary Table 2**), the bacterial genome was fragmented by Covaris 55 µL series Ultrasonicator and used to construct paired-end libraries with an insert size of 200-400 bp. Bacterial genomes were sequenced on the BGISEQ-500 (MGI, BGI-Shenzhen) platform, generating 1.4-2.0 Gb sequencing data for each sample with a sequencing depth >100x. Reads were checked for contamination using kraken2 (Wood et al., 2019) and only considered for further analysis if >90% of the reads identified as *P. aeruginosa*. Quality control of the raw data was performed using FastQC[49] with default parameters. For samples sequenced at MiGS, sequencing was performed as described above for phages. Reads obtained for all samples were assembled using Unicycler and the assembly quality was assessed using assembly-stats.v1.0.1 and BUSCO.v4[50] (pseudomonodales_odb10), and the GC% was calculated using bioawk. The sequencing depth was calculated using minimap2[51] and samtools mpileup[52,53].

Genome annotation

Bacterial genomes were annotated using prokka[54]. The genomes were used to determine the multi-locus sequence type (MLST) of the strains using the PubMLST website (https://pubmlst.org/)[55], and the serotype using the *Pseudomonas aeruginosa* serotyper PAst (https://github.com/Sandramses/PAst). Phage genomes were annotated using the RAST server[56], the start of the phage genome was determined using PhageTerm[57], and partial genes were manually verified and removed. The phage lifestyle was predicted using PhageAI[58].

Phage taxonomy and phylogenomics

Phages from our collection were classified taxonomically using GRAViTy[59]. In addition, VICTOR[60] was used to create phylogenetic trees for our phage collection and subsets thereof.

Detection of defense systems in bacterial genomes

Defense systems were detected in the genomes of the *P. aeruginosa* clinical isolates with PADLOC-DB v1.4.0[61], DefenseFinder[17], and the HMMs with completeness rules and thresholds as applied in Gao *et al* (2020)[29]. In addition, the representative sequences provided by Vassallo *et al* (2022)[14] were used to search for the defense systems described in this work. Homology searches were performed via blastp[62] (> 0.7 subject length / query length < 1.5 ; 0.7 > query coverage < 1.3; evalue < 1e-9; except for PD-T4-6: evalue < 1e-20). Systems were considered complete when all genes were present without more than 5 genes in between. In case of discrepancies between the algorithms, we considered the output reporting the most hits. For PADLOC, we excluded defense systems of the “other” categories. For DefenseFinder, we excluded results of defense systems that were not discriminated into subtypes, e.g. BREX.

In addition, a manual search of the neighborhood of the defense systems identified by the algorithms led to the identification of a variant of the TerY-P system that contained all three genes and corresponding functional domains of the original system[29]. The new TerY-P sequences were used to search for this variant in the bacterial genomes using blastp with evalue < 2.34e-29 and pident > 30. Systems were considered complete when all genes were present with less than 3 genes in between.

Pearson (pairwise.complete.obs) correlation was used from the corrr package in R[63] to determine the co-occurrence of defense systems in the *P. aeruginosa* genomes of the RefSeq database. P-values were adjusted with the Bonferroni method. Defense systems were considered to co-localize when having less than 50 genes in between for more than 50% of the instances in which they co-occur.

Detection of mobile genetic elements in bacterial genomes

PPanGGOLiN v1.2.74[64] was used to predict mobile genetic elements based on the regional genome plasticity of the *P. aeruginosa* genomes of the RefSeq database.

Detection of CRISPR-Cas I-F spacers targeting phages from our collection

Spacers were detected in the bacterial genomes using CRISPRDetect[65], and were mapped to our phage collection using blastn (word size = 8; evalue = 1; query coverage > 90; pident > 90; no gaps; maximum of 1 mismatch allowed). The PAM (5'-CC) was manually checked, with a +1 or -1 PAM slippage (5'-CN or 5'-NC) allowed. Spacers with a matching PAM and protospacer were categorized as interference-proficient, while spacers with a PAM slippage or up to five protospacer mutations (with correct PAM) were categorized as priming-proficient spacers.

Detection of anti-defense genes in bacteriophage and bacterial genomes

Acrs were detected using AcrFinder[40]. For the detection of anti-RM (*ardA*[37], *klcA*[38], *ardB*, *ocyA*, *ocr*, *darA*, *darB*[39], anti-CBASS Type I (*acb1*)[41], anti-CBASS Type II (*acbII*)[27], anti-Pycsar (*apyc*)[41] and anti-TIR-STING[42] genes, we first searched for *P. aeruginosa* homologs using PSI-BLAST[66] (maximum of 3 runs with 500 sequences; coverage > 60%, pident > 10%). Homolog functionality was checked using HMMer[67] and HHpred[68]. *P. aeruginosa* homologs were only found for anti-genes *acb1* and *acbII*. These homologs were searched for in our phage and bacterial genomes with the use of blastp (evalue < 10^-8 ; pident > 30 ; coverage > 60% ; 2.0 < subject length / query length > 0.5). For genes with no *P. aeruginosa* homologs, we created an HMM from the multiple alignment file obtained from the PSI-BLAST search above, using hmmbuild v3.3.2[67] with default settings. These HMMs were used to search for the anti-defense genes in our phage and bacterial collections (evalue < 10^-6). All hits obtained were checked for the presence of expected functional domains by HMMer and HHpred.

Cloning of defense systems in PAO1

Defense systems were amplified from *P. aeruginosa* strains using the primers indicated in **Supplementary Table 6** with Q5 DNA Polymerase (New England Biolabs), in reactions that added regions of homology to plasmid pUCP20. PCR products were run on 1% agarose gels and bands of the desired size were excised and cleaned using the Zymoclean Gel DNA Recovery Kit. Plasmid pUCP20 (pEmpty, **Supplementary Table 7**) was digested with BamHI and EcoRI, treated with FastAP (Thermo Scientific), and cleaned with the Zymo DNA Clean & Concentrator Kit. Each defense system was cloned into pEmpty using the NEBuilder HiFi DNA Assembly Master Mix, and transformed into chemically competent NEB® 5-alpha Competent *E. coli* following the manufacturer's instructions. Plasmids were extracted using the GeneJET

Plasmid Miniprep kit, confirmed by sequencing (Macrogen, primers in **Supplementary Table 6**), and electroporated into PAO1 as previously described[69]. Briefly, an overnight culture of PAO1 was centrifuged at 16,000 × *g* for 2 min at room temperature, and the pellet was washed twice and resuspended in 300 mM of sucrose. The suspension was mixed with 100-500 ng of plasmid DNA and electroporated at 2.5 kV in a 2 mm gap electroporation cuvette. Cells were recovered in LB for 1-2 h at 37 °C and plated in LBA plates supplemented with 200 µg/ml of carbenicillin.

Efficiency of plating

The 10^8 pfu/ml phage stocks were 10-fold serially diluted in LB and the dilutions were spotted onto DLA plates of PAO1, or DLA+carbenicillin plates of PAO1 with pEmpty or PAO1 with individual defense systems following the small plaque drop assay[70]. The phage dilution that resulted in countable phage plaques was used in double-layer overlay plaque assays[71] with PAO1, PAO1 with pEmpty, or PAO1 with the defense systems. The anti-phage activity of the systems was determined as the fold reduction in phage plaques in comparison to the number of plaques obtained in the PAO1:pEmpty control. The diameter of the phage plaques was measured to determine differences in plaque size caused by the defense systems.

Infection dynamics of phage-infected cultures

Bacterial cultures of PAO1 with pEmpty or with individual defense systems were grown to early exponential phase (OD_{600} ≈ 0.3) and infected with phage at an MOI of >1. The cultures were incubated at 37°C with rocking, and samples were taken at 0h, 2h, and 4h to measure phage and bacteria concentration. The sample was centrifuged at 9,000 × *g* for 2 min, and the phage-containing supernatant was 10-fold serially diluted and spotted onto DLA plates of PAO1 to estimate phage concentration. The pellet was washed twice with LB, 10-fold serially diluted, and spotted onto LBA plates to determine bacterial concentration.

Liquid culture collapse assays

Overnight grown bacteria were diluted to an OD_{600} of approximately 0.1 in LB media. The cell suspension was distributed into the wells of 96-well plates, and phages were added at MOIs of 10, 0.1, 0.01, and 0.001). Assays were performed in triplicates. The plates were incubated at 37°C in an Epoch2 microplate spectrophotometer (Biotek) for OD_{600} measurements every 10 min for 24h, with double orbital shaking. Curves obtained at high and low MOI were compared to those of the infected control, and the effect was classified as 1) protection, when the system protects against phage infection at high and low MOI, 2) classic abortive infection, when the system protects against phage infection only at low MOI, 3) population-wide abortive

infection when the system causes growth arrest at both high and low MOI, and 4) no protection, when the system has no effect.

Fluorescence microscopy of defense systems

Exponentially growing (OD_{600} ≈ 0.3) cultures of PAO1 strains containing pEmpty or the defense systems were infected with phage at an MOI of ≥ 3, and the phage was adsorbed for 10 min at 37 °C. Cells were centrifuged at 9,000 × *g* for 1 min, and the cell pellet was re-suspended in 5 µL of 1 µM of propidium iodide. The stained cells were spotted onto 1% agarose pads[72], and visualized using a Nikon Eclipse Ti2 inverted fluorescence microscope equipped with a 100× oil immersion objective (Nikon Apo TIRF; 1.49 numerical aperture). Time-lapse phase-contrast (CD Retiga R1) and fluorescence images (after excitation with a 561 nm laser 2000 609/54 bandpass filter, EM-CCD Andor iXON Ultra 897) were acquired every 5 min using Metamorph.

Statistical analysis

Unless stated otherwise, data are presented as the mean of biological triplicates ± standard deviation. Correlation between the number of defense systems and phage resistance was determined by linear regression models using the lm function of R. Co-occurrence of defense systems was determined using the Pearson (pairwise.complete.obs) correlation from the corrr package in R. P-values were adjusted with the Bonferroni method.

Data availability

All data supporting the findings of this study are available within the paper, in the Supplementary Data, and at https://github.com/BrounsLab-TUDelft/Pseudomonas_Defence_Systems. All original code has been deposited at Github. Raw data and assembled bacterial and phage genomes are available from Genbank, Bioproject PRJNA817167 (individual accession numbers are listed in Supplementary Tables 2 and 3). All unique bacterial strains, phages, and plasmids generated in this study are available from the corresponding author upon request.

Acknowledgements

We thank Linyi Gao and Feng Zhang (Massachusetts Institute of Technology) for kindly providing the HMMs for the detection of defense systems, and Wenchen Song and Minfeng Xiao (BGI-Shenzhen) for sequencing part of the clinical isolates and phages used in this study.

We would like to thank Wim de Leeuw and Han Rauwerda (University of Amsterdam, Swammerdam Institute for Life Sciences, MAD/RB&AB) for the use of the Crunchomics computer cluster. We also thank members of the Brounslab for the many discussions and ideas that improved our work. This work was supported by grants from the European Research Council (ERC) CoG under the European Union's Horizon 2020 research and innovation program (grant agreement No. 101003229) and the Netherlands Organisation for Scientific Research (NWO VICI; VI.C.192.027) to S.J.J.B.

Author contributions

Conceptualization, S.J.J.B.; Methodology; S.J.J.B., F.L.N, A.R.C., and D.F.B.; Software, D.F.B. and A.M.; Formal Analysis, A.R.C., D.F.B., J.Q.E., A.M., B.A.S., and H.B.; Investigation, A.R.C., D.F.B., J.Q.E., A.M., H.B, B.E.B., A.C.H.; Visualization, A.R.C., D.F.B., J.Q.E., H.B., and A.M.; Data Curation, A.R.C., D.F.B., and J.Q.E.; Writing – Original Draft, A.R.C., D.F.B, and J.Q.E.; Writing – Review & Editing, S.J.J.B.; Resources, P.J.H., F.L.N.; Funding Acquisition, S.J.J.B.

Declaration of interests

The authors declare no competing interests.

Figure legends

Fig. 1 | Defense systems are abundant and diverse in *P. aeruginosa* strains. a, Diversity of defense systems found in the genomes of 315 *P. aeruginosa* strains from the RefSeq database, organized and colored in a gradient from most (left) to least (right) abundant. Only the 58 most prevalent defense systems are shown (see **Supplementary Table 1** for the full list of 117 defense systems). **b,** Number of defense systems per genome in *P. aeruginosa* strains from the RefSeq database. The median number of defense systems is shown in red. **c,** Diversity of defense systems found in the genomes of 17 clinical isolates of *P. aeruginosa* from our collection. Systems are organized from most (left) to least (right) prevalent and colored according to the abundance in (**a**). Systems present in the clinical isolates but not in the RefSeq database are colored white. All 58 defense systems found in the clinical strains are shown. **d,** Number of defense systems per genome in *P. aeruginosa* strains from our collection of clinical isolates. The median number of defense systems is shown in red.

Fig. 2 | Innate and adaptive defense systems correlate with phage resistance. a, Host range of phages against 17 clinical isolates of *P. aeruginosa* and strain PAO1. Phages are clustered by phylogeny (**Supplementary Table 3**). Phage-bacteria interactions are depicted as infection (dark blue), strong adsorption (>70%) but no infection (medium blue), weak adsorption (50-70%) but no infection (light blue), or no interaction (white). Cases of infection in which the phage carries an anti-gene for a defense present in the strain are indicated with a star. Instances in which a strain carries a spacer targeting phages from the panel are indicated as a white circle for interference-proficient CRISPR-Cas spacers (i.e., spacers with matching protospacer adjacent motif (PAM) and protospacer) or as a blue circle for priming-proficient spacers (i.e., spacers with a ±1 slipped PAM or up to 5 protospacer mutations). For each phage, the percentage of strains infected (I) compared to those the phage can interact with (adsorb and infect, A+I) is indicated at the bottom as % I/(A+I). **b,** Number of defense systems found in the *P. aeruginosa* clinical isolates correlates with the levels of phage resistance. Phage infection is here portrayed as the percentage of adsorbing phages that can establish a productive infection (% $\phi_{Infecting}$ / ($\phi_{Adsorbing}$+$\phi_{Infecting}$)). Dark blue represents infection, and light blue represents adsorption. Strains are vertically sorted based on number of defense systems detected. **c,** Defense systems found in the *P. aeruginosa* clinical isolates. The number of instances of each system type per strain is indicated in yellow, orange, or red for 1, 2, or 3 respectively. The total number of defense systems found per strain is indicated in a heatmap bar on the right.

Fig. 3 | **Defense systems provide morphotype-specific anti-phage activity. a,** Efficiency of plating (EOP) of phages in PAO1 containing individual defense systems. EOP was determined as the fold decrease of phage titer in the strain with the defense system compared to the titer obtained in the strain without the defense system. An example of fold decrease with *qatABCD*-containing cells and myophage ϕPa33 is shown on top. Plaque size reductions of phages plated in PAO1 containing individual defense systems as compared to a control without a system are indicated as a colored corner. Examples of plaque size decrease observed for podophage ϕPa3, siphophage ϕPa28, and myophage ϕPa33 with QatABCD cells are shown on top. **b,** Liquid culture collapse assays of PAO1 containing individual defense systems (DS) infected with phages, as compared to a control (WT) without a defense system. Results are shown as a summary of the effects observed when infecting the cultures with an MOI of 10 and with MOI of 0.01. The effect is represented as protection (blue) when cells are protected from phage infection at high and low MOIs, as classic abortive infection when cells are protected from phage infection at low MOI, and as population-wide abortive infection when growth arrest is observed at both high and low MOIs. Illustrations of growth curves obtained for each category are shown on top. **c,** Time-lapse phase contrast and fluorescence images of PAO1 cells containing individual defense systems infected with phage. Cells were stained with propidium iodide to visualize permeabilization of the cell membrane due to cell death. CBASS Type III cells infected with phage ϕPa25 show cell death but less released DNA than in control cells, likely due to degradation of both phage and host DNA by the effector NucC (**Supplementary Fig. 1a**), as previously described in *E. coli* [73]. TerY-P and Zorya Type I cells survive phage infection, although some cell death is still observed for TerY-P, consistent with the EOP results in **a**.

Fig. 4 | **Co-occurrence and co-localization of defense systems for broader anti-phage activity. a,** PCA plot of defense system co-occurrence within the complete *P. aeruginosa* genomes of the RefSeq database (n = 315). Co-occurrences with a Pearson correlation coefficient (r) < 0.25 are shown as dotted lines and those larger than 0.25 are indicated by the thickness of the line. Co-localizing systems are shown in red. **b,** Hypothetical model for the broad, complementary anti-phage defense provided by the combination of Druantia Type III, TerY-P, Wadjet Type I, RM Type I, and Mokosh Type I. Questions marks represent unknown specificities for systems not tested here. **c,** Genomic integration hotspot in *P. aeruginosa* L0872 containing modules of defense genes that include the co-occurring Wadjet Type I, Druantia Type III, TerY-P, RM Type I, and Mokosh Type I.

Supplementary Information

Supplementary Fig. 1 | Individual defense systems cloned in *Pseudomonas aeruginosa* strain PAO1.

Supplementary Table 1 | Matrix of defense systems identified in the 315 RefSeq genomes of *Pseudomonas aeruginosa*.

Supplementary Table 2 | Features of the clinical isolates of *Pseudomonas aeruginosa* used in this work, including defense system presence.

Supplementary Table 3 | Features of the *Pseudomonas aeruginosa* phages used in this study.

Supplementary Table 4 | List of CRISPR-Cas Type I-F interference-proficient and priming-proficient spacers found in the clinical isolates of *Pseudomonas aeruginosa* to target phages from our collection.

Supplementary Table 5 | Co-occurrence and co-localization of defense systems in the *Pseudomonas aeruginosa* genomes of the RefSeq database.

Supplementary Table 6 | List of primers used in this work.

Supplementary Table 7 | List of plasmids used in this work.

References

1 Piel, D. *et al.* Phage–host coevolution in natural populations. *Nat Microbiol* 7, 1075-1086 (2022).

2 Burmeister, A. R. *et al.* Pleiotropy complicates a trade-off between phage resistance and antibiotic resistance. *Proc Natl Acad Sci U S A* **117**, 11207-11216 (2020).

3 Labrie, S. J., Samson, J. E. & Moineau, S. Bacteriophage resistance mechanisms. *Nat Rev Microbiol* **8**, 317-327 (2010).

4 Bernheim, A. & Sorek, R. The pan-immune system of bacteria: antiviral defence as a community resource. *Nat Rev Microbiol* **18**, 113-119 (2020).

5 Hampton, H. G., Watson, B. N. J. & Fineran, P. C. The arms race between bacteria and their phage foes. *Nature* **577**, 327-336 (2020).

6 Egido, J. E., Costa, A. R., Aparicio-Maldonado, C., Haas, P.-J. & Brouns, S. J. J. Mechanisms and clinical importance of bacteriophage resistance. *FEMS Microbiol Rev* **46**, fuab048 (2022).

7 Barrangou, R. *et al.* CRISPR Provides Acquired Resistance Against Viruses in Prokaryotes. *Science* **315**, 1709-1712 (2007).

8 Mohanraju, P. *et al.* Diverse evolutionary roots and mechanistic variations of the CRISPR-Cas systems. *Science* **353**, aad5147 (2016).

9 Bickle, T. A. Restricting restriction. *Mol Microbiol* **51**, 3-5 (2004).

10 Dussoix, D. & Arber, W. Host specificity of DNA produced by Escherichia coli: II. Control over acceptance of DNA from infecting phage λ. *J Mol Biol* **5**, 37-49 (1962).

11 Koonin, E. V., Makarova, K. S. & Wolf, Y. I. Evolutionary Genomics of Defense Systems in Archaea and Bacteria. *Annu Rev Microbiol* **71**, 233-261 (2017).

12 Tal, N. & Sorek, R. SnapShot: Bacterial immunity. *Cell* **185**, 578-578.e571 (2022).

13 Millman, A. *et al.* An expanding arsenal of immune systems that protect bacteria from phages. *bioRxiv*, 2022.2005.2011.491447 (2022).

14 Vassallo, C., Doering, C., Littlehale, M. L., Teodoro, G. & Laub, M. T. Mapping the landscape of anti-phage defense mechanisms in the E. coli pangenome. *bioRxiv*, 2022.2005.2012.491691 (2022).

15 Hussain, F. A. *et al.* Rapid evolutionary turnover of mobile genetic elements drives bacterial resistance to phages. *Science* **374**, 488-492 (2021).

16 Rousset, F. *et al.* Phages and their satellites encode hotspots of antiviral systems. *Cell Host Microbe* **30**, 740-753.e745 (2022).

17 Tesson, F. *et al.* Systematic and quantitative view of the antiviral arsenal of prokaryotes. *Nat Commun* **13**, 2561 (2022).

18 Krylov, V. *et al.* Phage phiKZ-The First of Giants. *Viruses* **13**, 149 (2021).

19 Jackson, S. A., Birkholz, N., Malone, L. M. & Fineran, P. C. Imprecise Spacer Acquisition Generates CRISPR-Cas Immune Diversity through Primed Adaptation. *Cell Host Microbe* **25**, 250-260.e254 (2019).

20 Fineran, P. C. *et al.* Degenerate target sites mediate rapid primed CRISPR adaptation. *Proc Natl Acad Sci U S A* **111**, E1629-E1638 (2014).

21 Staals, R. H. J. *et al.* Interference-driven spacer acquisition is dominant over naive and primed adaptation in a native CRISPR–Cas system. *Nat Commun* **7**, 12853 (2016).

22 Cady, K. C. *et al.* Prevalence, conservation and functional analysis of Yersinia and Escherichia CRISPR regions in clinical Pseudomonas aeruginosa isolates. *Microbiology* **157**, 430-437 (2011).

23 Li, Y. & Bondy-Denomy, J. Anti-CRISPRs go viral: The infection biology of CRISPR-Cas inhibitors. *Cell Host Microbe* **29**, 704-714 (2021).

24 Malone, L. M., Birkholz, N. & Fineran, P. C. Conquering CRISPR: how phages overcome bacterial adaptive immunity. *Curr Opin Biotechnol* **68**, 30-36 (2021).

25 Schweizer, H. P. Escherichia-Pseudomonas shuttle vectors derived from pUC18/19. *Gene* **97**, 109-112 (1991).

26 Gao, L. A. *et al.* Prokaryotic innate immunity through pattern recognition of conserved viral proteins. *Science* **377**, eabm4096 (2022).

27 Huiting, E. *et al.* Bacteriophages antagonize cGAS-like immunity in bacteria. *bioRxiv*, 2022.2003.2030.486325 (2022).

28 Zhang, T. *et al.* Direct activation of an innate immune system in bacteria by a viral capsid protein. *bioRxiv*, 2022.2005.2030.493996 (2022).

29 Gao, L. *et al.* Diverse enzymatic activities mediate antiviral immunity in prokaryotes. *Science* **369**, 1077-1084 (2020).

30 Lopatina, A., Tal, N. & Sorek, R. Abortive Infection: Bacterial Suicide as an Antiviral Immune Strategy. *Annual Review of Virology* **7**, 371-384 (2020).

31 Doron, S. *et al.* Systematic discovery of antiphage defense systems in the microbial pangenome. *Science* **359**, eaar4120 (2018).

32 Bru, J.-L. *et al.* PQS Produced by the Pseudomonas aeruginosa Stress Response Repels Swarms Away from Bacteriophage and Antibiotics. *J Bacteriol* **201**, e00383-00319 (2019).

33 Høyland-Kroghsbo, N. M. *et al.* Quorum sensing controls the Pseudomonas aeruginosa CRISPR-Cas adaptive immune system. *Proc Natl Acad Sci U S A* **114**, 131-135 (2017).

34 Chaikeeratisak, V. *et al.* Assembly of a nucleus-like structure during viral replication in bacteria. *Science* **355**, 194-197 (2017).

35 Malone, L. M. *et al.* A jumbo phage that forms a nucleus-like structure evades CRISPR–Cas DNA targeting but is vulnerable to type III RNA-based immunity. *Nature Microbiology* **5**, 48-55 (2020).

36 Mendoza, S. D. *et al.* A bacteriophage nucleus-like compartment shields DNA from CRISPR nucleases. *Nature* **577**, 244-248 (2020).

37 McMahon, S. A. *et al.* Extensive DNA mimicry by the ArdA anti-restriction protein and its role in the spread of antibiotic resistance. *Nucleic Acids Res* **37**, 4887-4897 (2009).

38 Liang, W. *et al.* Anti-Restriction Protein, KlcAHS, Promotes Dissemination of Carbapenem Resistance. *Front Cell Infect Microbiol* **7** (2017).

39 Serfiotis-Mitsa, D. *et al.* The structure of the KlcA and ArdB proteins reveals a novel fold and antirestriction activity against Type I DNA restriction systems in vivo but not in vitro. *Nucleic Acids Res* **38**, 1723-1737 (2010).

40 Yi, H. *et al.* AcrFinder: genome mining anti-CRISPR operons in prokaryotes and their viruses. *Nucleic Acids Res* **48**, W358-W365 (2020).

41 Hobbs, S. J. *et al.* Phage anti-CBASS and anti-Pycsar nucleases subvert bacterial immunity. *Nature* **605**, 522-526 (2022).

42 Ho, P., Chen, Y., Biswas, S., Canfield, E. & Feldman, D. E. Bacteriophage anti-defense genes that neutralize TIR and STING immune responses. *bioRxiv*, 2022.2006.2009.495361 (2022).

43 Jaskólska, M., Adams, D. W. & Blokesch, M. Two defence systems eliminate plasmids from seventh pandemic Vibrio cholerae. *Nature* **604**, 323-329 (2022).

44 Wang, S. *et al.* The complex roles of genomic DNA modifications of bacteriophage T4 in resistance to nuclease-based defense systems of E. coli. *bioRxiv*, 2022.2006.2016.496414 (2022).

45 Nobrega, F. L. *et al.* Targeting mechanisms of tailed bacteriophages. *Nat Rev Microbiol* **16**, 760-773 (2018).

46 Abedon, S. T. Lysis from without. *Bacteriophage* **1**, 46-49 (2011).

47 Wick, R. R., Judd, L. M., Gorrie, C. L. & Holt, K. E. Unicycler: Resolving bacterial genome assemblies from short and long sequencing reads. *PLoS Comput Biol* **13**, e1005595 (2017).

48 Wick, R. R., Schultz, M. B., Zobel, J. & Holt, K. E. Bandage: interactive visualization of de novo genome assemblies. *Bioinformatics* **31**, 3350-3352 (2015).

49 Andrews, S. FastQC: a quality control tool for high throughput sequence data, http://www.bioinformatics.babraham.ac.uk/projects/fastqc (2010).

50 Simão, F. A., Waterhouse, R. M., Ioannidis, P., Kriventseva, E. V. & Zdobnov, E. M. BUSCO: assessing genome assembly and annotation completeness with single-copy orthologs. *Bioinformatics* **31**, 3210-3212 (2015).

51 Li, H. Minimap2: pairwise alignment for nucleotide sequences. *Bioinformatics* **34**, 3094-3100 (2018).

52 Danecek, P. *et al.* Twelve years of SAMtools and BCFtools. *GigaScience* **10**, giab008 (2021).

53 Li, H. *et al.* The Sequence Alignment/Map format and SAMtools. *Bioinformatics* **25**, 2078-2079 (2009).

54 Seemann, T. Prokka: rapid prokaryotic genome annotation. *Bioinformatics* **30**, 2068-2069 (2014).

55 Jolley, K. A. & Maiden, M. C. J. BIGSdb: Scalable analysis of bacterial genome variation at the population level. *BMC Bioinf* **11**, 595 (2010).

56 Aziz, R. K. *et al.* The RAST Server: rapid annotations using subsystems technology. *BMC genomics* **9**, 75-75 (2008).

57 Garneau, J. R., Depardieu, F., Fortier, L.-C., Bikard, D. & Monot, M. PhageTerm: a tool for fast and accurate determination of phage termini and packaging mechanism using next-generation sequencing data. *Sci Rep* **7**, 8292 (2017).

58 Tynecki, P. *et al.* PhageAI - Bacteriophage Life Cycle Recognition with Machine Learning and Natural Language Processing. *bioRxiv*, 2020.2007.2011.198606 (2020).

59 Aiewsakun, P., Adriaenssens, E. M., Lavigne, R., Kropinski, A. M. & Simmonds, P. Evaluation of the genomic diversity of viruses infecting bacteria, archaea and eukaryotes using a common bioinformatic platform: steps towards a unified taxonomy. *J Gen Virol* **99**, 1331-1343 (2018).

60 Meier-Kolthoff, J. P. & Göker, M. VICTOR: genome-based phylogeny and classification of prokaryotic viruses. *Bioinformatics* **33**, 3396-3404 (2017).

61 Payne, L. J. *et al.* Identification and classification of antiviral defence systems in bacteria and archaea with PADLOC reveals new system types. *Nucleic Acids Res* **49**, 10868-10878 (2021).

62 Altschul, S. F., Gish, W., Miller, W., Myers, E. W. & Lipman, D. J. Basic local alignment search tool. *J Mol Biol* **215**, 403-410 (1990).

63 R: A language and environment for statistical computing (R Foundation for Statistical Computing, Vienna, Austria, 2018).

64 Gautreau, G. *et al.* PPanGGOLiN: Depicting microbial diversity via a partitioned pangenome graph. *PLoS Comput Biol* **16**, e1007732 (2020).

65 Biswas, A., Staals, R. H. J., Morales, S. E., Fineran, P. C. & Brown, C. M. CRISPRDetect: A flexible algorithm to define CRISPR arrays. *BMC Genom* **17**, 356-356 (2016).

66 Altschul, S. F. *et al.* Gapped BLAST and PSI-BLAST: a new generation of protein database search programs. *Nucleic Acids Res* **25**, 3389-3402 (1997).

67 Finn, R. D., Clements, J. & Eddy, S. R. HMMER web server: interactive sequence similarity searching. *Nucleic Acids Res* **39**, W29-W37 (2011).

68 Söding, J., Biegert, A. & Lupas, A. N. The HHpred interactive server for protein homology detection and structure prediction. *Nucleic Acids Res* **33**, W244-W248 (2005).

69 Choi, K.-H., Kumar, A. & Schweizer, H. P. A 10-min method for preparation of highly electrocompetent Pseudomonas aeruginosa cells: Application for DNA fragment transfer between chromosomes and plasmid transformation. *J Microbiol Meth* **64**, 391-397 (2006).

70 Mazzocco, A., Waddell, T. E., Lingohr, E. & Johnson, R. P. in *Bacteriophages: Methods and Protocols, Volume 1: Isolation, Characterization, and Interactions* (eds Martha R. J. Clokie & Andrew M. Kropinski) 81-85 (Humana Press, 2009).

71 Kropinski, A. M., Mazzocco, A., Waddell, T. E., Lingohr, E. & Johnson, R. P. in *Bacteriophages: Methods and Protocols, Volume 1: Isolation, Characterization, and Interactions* (eds Martha R. J. Clokie & Andrew M. Kropinski) 69-76 (Humana Press, 2009).

72 Vink, J. N. A., Brouns, S. J. J. & Hohlbein, J. Extracting Transition Rates in Particle Tracking Using Analytical Diffusion Distribution Analysis. *Biophys J* **119**, 1970-1983 (2020).

73 Lau, R. K. *et al.* Structure and Mechanism of a Cyclic Trinucleotide-Activated Bacterial Endonuclease Mediating Bacteriophage Immunity. *Mol Cell* **77**, 723-733.e726 (2020).

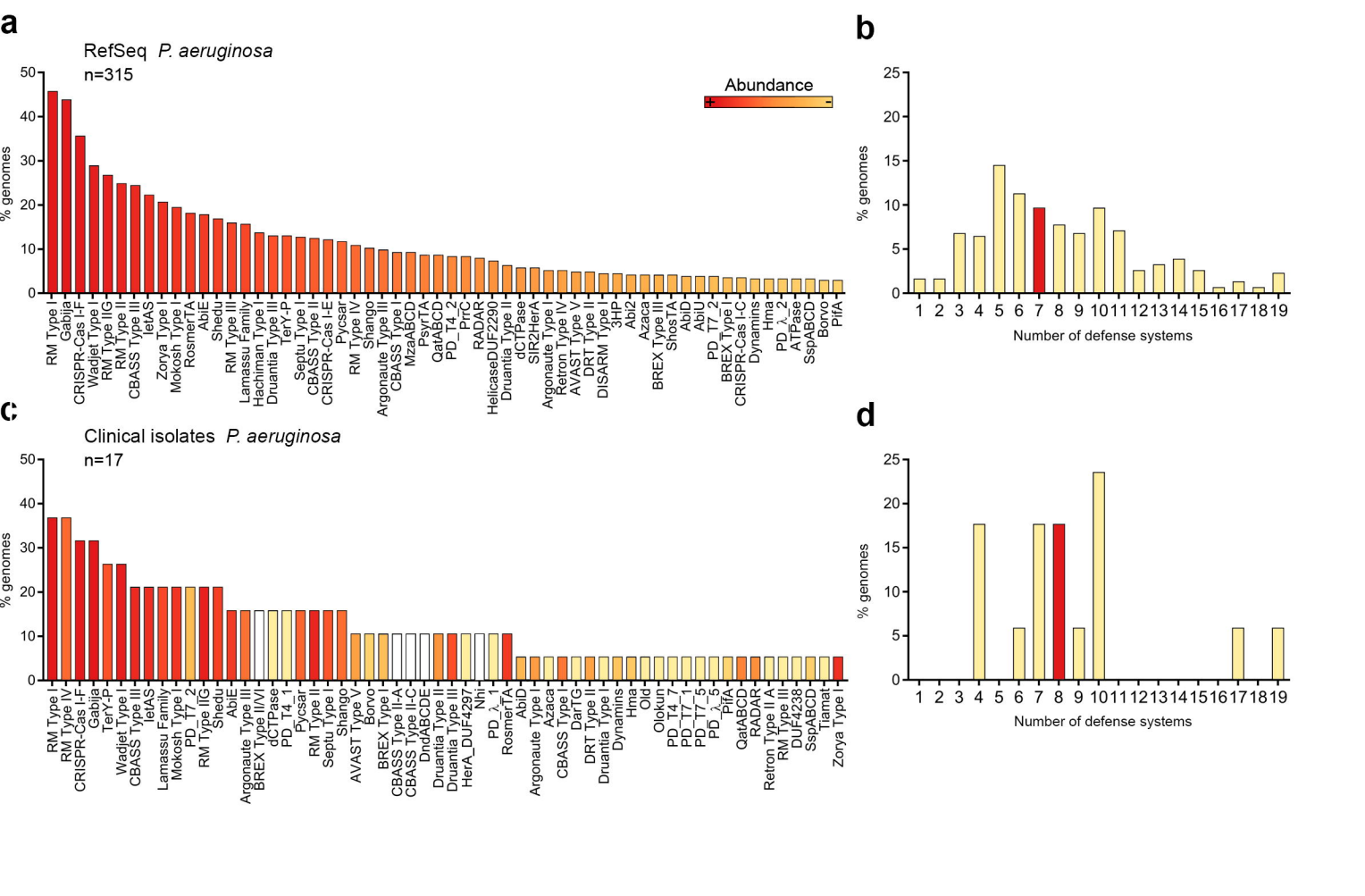
a
RefSeq P. aeruginosa
n=315
Abundance
+
-
% genomes
0
10
20
30
40
50
RM Type I
Gabija
CRISPR-Cas I-F
Wadjet Type I
RM Type IIG
RM Type II
CBASS Type III
JetAS
Zorya Type I
Mokosh Type I
RosmerTA
AbiE
Shedu
RM Type III
Lamassu Family
Hachiman Type I
Druantia Type III
TerY-P
Septu Type I
CBASS Type II
CRISPR-Cas I-E
Pycsar
RM Type IV
Shango
Argonaute Type III
CBASS Type I
MzaABCD
PsyrTA
QatABCD
PD_T4_2
PrrC
RADAR
HelicaseDUF2290
Druantia Type II
dCTPase
SIR2HerA
Argonaute Type I
Retron Type IV
AVAST Type V
DRT Type II
DISARM Type I
3HP
Abi2
Azaca
BREX Type III
ShosTA
AbiD
AbiU
PD_T7_2
BREX Type I
CRISPR-Cas I-C
Dynamins
Hma
PD_λ_2
ATPase
SspABCD
Borvo
PifA
b
% genomes
0
5
10
15
20
25
1 2 3 4 5 6 7 8 9 10 11 12 13 14 15 16 17 18 19
Number of defense systems
c
Clinical isolates P. aeruginosa
n=17
% genomes
0
10
20
30
40
50
RM Type I
RM Type IV
CRISPR-Cas I-F
Gabija
TerY-P
Wadjet Type I
CBASS Type III
JetAS
Lamassu Family
Mokosh Type I
PD_T7_2
RM Type IIG
Shedu
AbiE
Argonaute Type III
BREX Type II/VI
dCTPase
PD_T4_1
Pycsar
RM Type II
Septu Type I
Shango
AVAST Type V
Borvo
BREX Type I
CBASS Type II-A
CBASS Type II-C
DndABCDE
Druantia Type II
Druantia Type III
HerA_DUF4297
Nhi
PD_λ_1
RosmerTA
AbiD
Argonaute Type I
Azaca
CBASS Type I
DarTG
DRT Type II
Druantia Type I
Dynamins
Hma
Old
Olokun
PD_T4_7
PD_T7_1
PD_T7_5
PD_λ_5
PifA
QatABCD
RADAR
Retron Type II A
RM Type III
DUF4238
SspABCD
Tiamat
Zorya Type I
d
% genomes
0
5
10
15
20
25
1 2 3 4 5 6 7 8 9 10 11 12 13 14 15 16 17 18 19
Number of defense systems

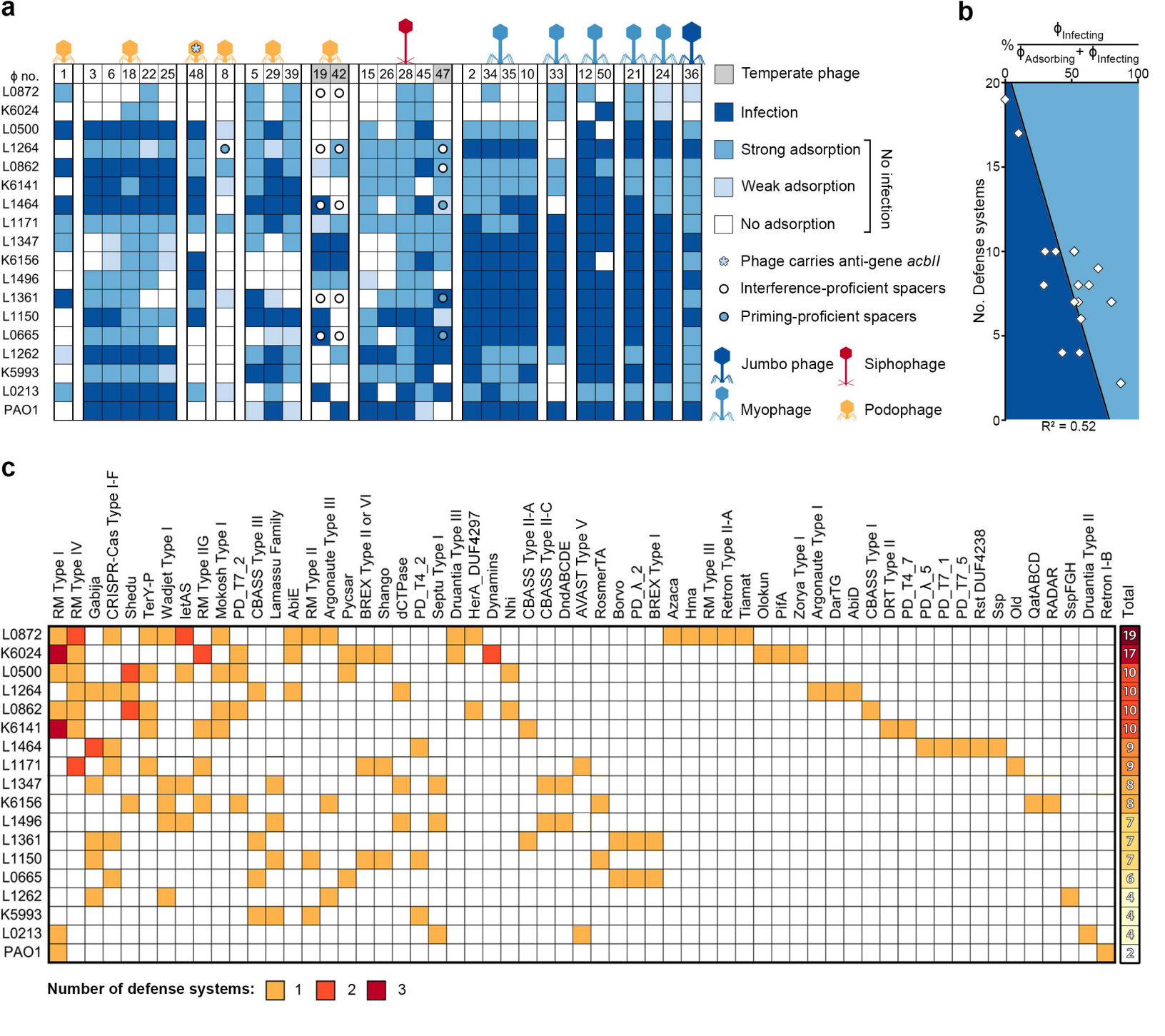
a
ϕ no.
1
3
6
18
22
25
48
8
5
29
39
19
42
15
26
28
45
47
2
34
35
10
33
12
50
21
24
36
L0872
K6024
L0500
L1264
L0862
K6141
L1464
L1171
L1347
K6156
L1496
L1361
L1150
L0665
L1262
K5993
L0213
PAO1
Temperate phage
Infection
Strong adsorption
Weak adsorption
No adsorption
No infection
Phage carries anti-gene acbII
Interference-proficient spacers
Priming-proficient spacers
Jumbo phage
Siphophage
Myophage
Podophage
b
% ϕInfecting / ϕAdsorbing + ϕInfecting
0
50
100
20
15
10
5
0
No. Defense systems
R² = 0.52
c
RM Type I
RM Type IV
Gabija
CRISPR-Cas Type I-F
Shedu
TerY-P
Wadjet Type I
letAS
RM Type IIG
Mokosh Type I
PD_T7_2
CBASS Type III
Lamassu Family
AbiE
RM Type II
Argonaute Type III
Pycsar
BREX Type II or VI
Shango
dCTPase
PD_T4_2
Septu Type I
Druantia Type III
HerA_DUF4297
Dynamins
Nhi
CBASS Type II-A
CBASS Type II-C
DndABCDE
AVAST Type V
RosmerTA
Borvo
PD_λ_2
BREX Type I
Azaca
Hma
RM Type III
Retron Type II-A
Tiamat
Olokun
PifA
Zorya Type I
Argonaute Type I
DarTG
AbiD
CBASS Type I
DRT Type II
PD_T4_7
PD_λ_5
PD_T7_1
PD_T7_5
Rst DUF4238
Ssp
Old
QatABCD
RADAR
SspFGH
Druantia Type II
Retron I-B
Total
L0872 19
K6024 17
L0500 10
L1264 10
L0862 10
K6141 10
L1464 9
L1171 9
L1347 8
K6156 8
L1496 7
L1361 7
L1150 7
L0665 6
L1262 4
K5993 4
L0213 4
PAO1 2
Number of defense systems: 1 2 3

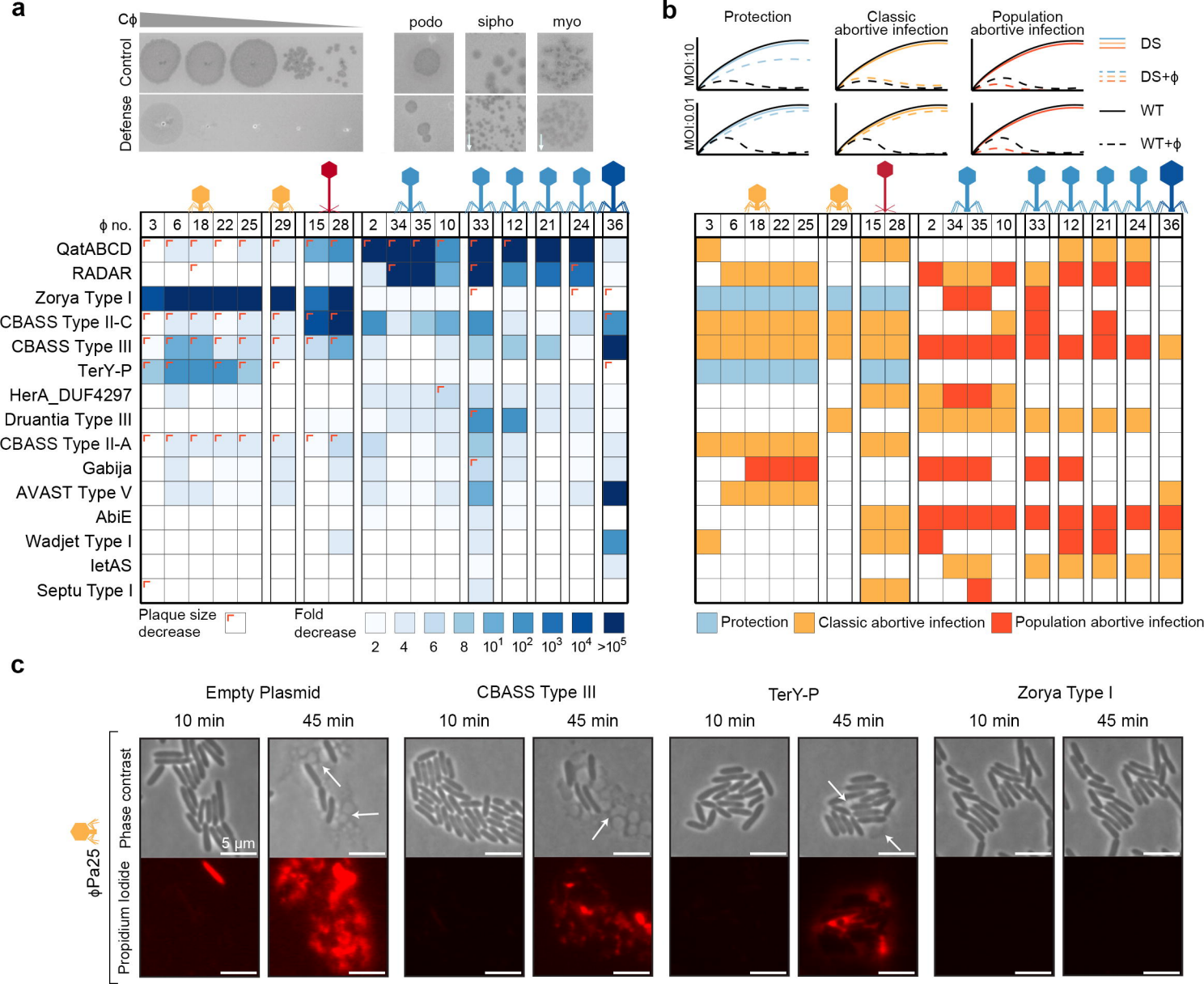
a
Cϕ
Control
Defense
podo
sipho
myo
ϕ no.
3 6 18 22 25 29 15 28 2 34 35 10 33 12 21 24 36
QatABCD
RADAR
Zorya Type I
CBASS Type II-C
CBASS Type III
TerY-P
HerA_DUF4297
Druantia Type III
CBASS Type II-A
Gabija
AVAST Type V
AbiE
Wadjet Type I
IetAS
Septu Type I
Plaque size decrease
Fold decrease
2 4 6 8 10^1 10^2 10^3 10^4 >10^5
b
Protection
Classic abortive infection
Population abortive infection
MOI:10
MOI:0.01
DS
DS+ϕ
WT
WT+ϕ
3 6 18 22 25 29 15 28 2 34 35 10 33 12 21 24 36
Protection
Classic abortive infection
Population abortive infection
c
Empty Plasmid
CBASS Type III
TerY-P
Zorya Type I
10 min
45 min
ϕPa25
Phase contrast
Propidium Iodide
5 μm

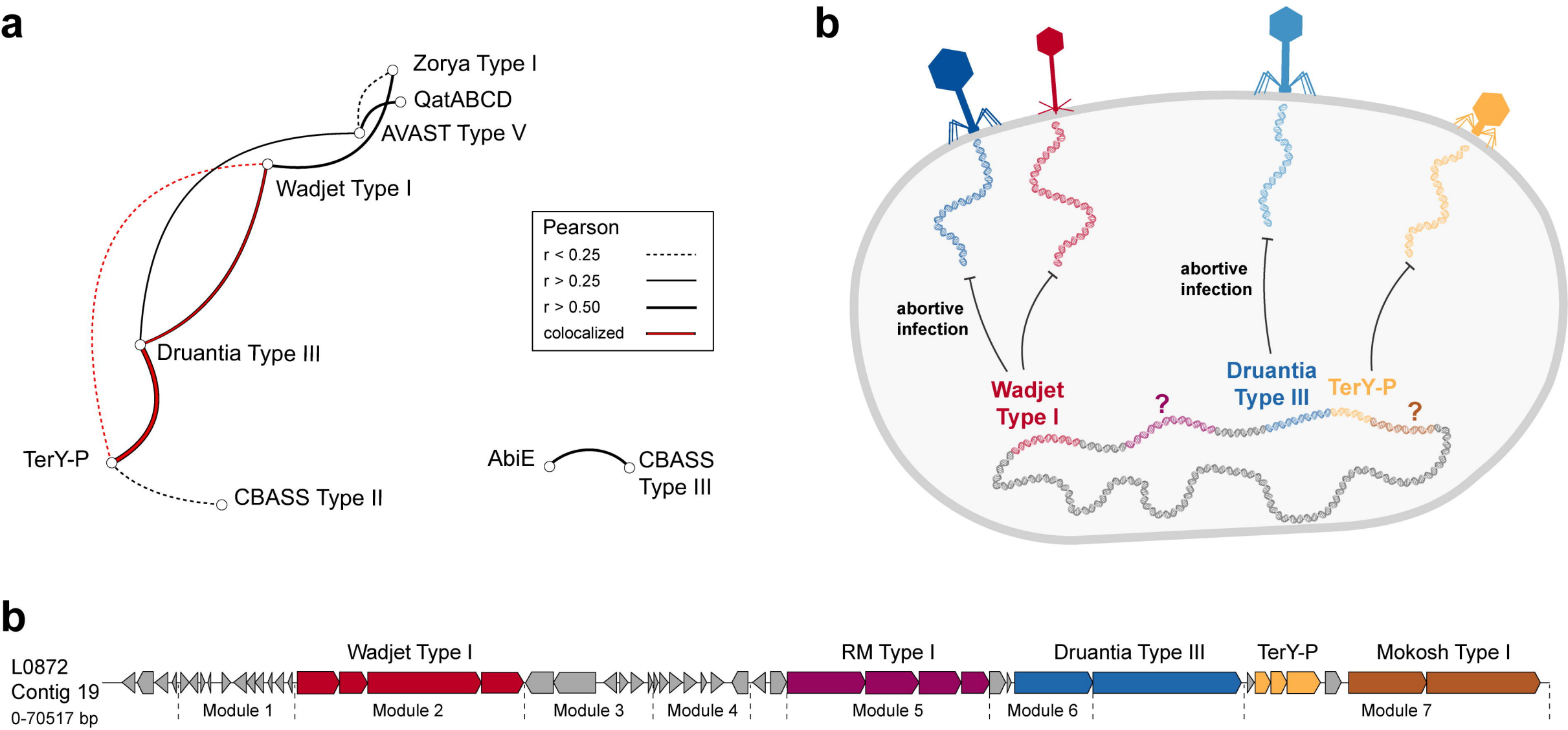
a
Zorya Type I
QatABCD
AVAST Type V
Wadjet Type I
Druantia Type III
TerY-P
CBASS Type II
Pearson
r < 0.25
r > 0.25
r > 0.50
colocalized
AbiE
CBASS Type III
b
abortive infection
abortive infection
Wadjet Type I
Druantia Type III
TerY-P
?
?
b
L0872 Contig 19
0-70517 bp
Wadjet Type I
RM Type I
Druantia Type III
TerY-P
Mokosh Type I
Module 1
Module 2
Module 3
Module 4
Module 5
Module 6
Module 7